



## OPEN ACCESS

## EDITED BY

Santosh Kumar,  
KL University, India

## REVIEWED BY

Mandeep Singh,  
National Institute of Technology, India  
Sushank Chaudhary,  
Guangdong University of Petrochemical  
Technology, China

## \*CORRESPONDENCE

Mardeni Roslee,  
✉ mardeni.roslee@mmu.edu.my  
Farman Ali,  
✉ farmanali@nuua.edu.cn

RECEIVED 30 January 2025

ACCEPTED 14 April 2025

PUBLISHED 30 May 2025

## CITATION

Ullah R, Ali F, Armghan A, Afsar H,  
Alshamrani A and Roslee M (2025) Integrating  
MIMO and RoF technologies for low-latency  
and high-capacity 5G networks.  
*Front. Phys.* 13:1568555.  
doi: 10.3389/fphy.2025.1568555

## COPYRIGHT

© 2025 Ullah, Ali, Armghan, Afsar, Alshamrani  
and Roslee. This is an open-access article  
distributed under the terms of the [Creative  
Commons Attribution License \(CC BY\)](#). The  
use, distribution or reproduction in other  
forums is permitted, provided the original  
author(s) and the copyright owner(s) are  
credited and that the original publication in  
this journal is cited, in accordance with  
accepted academic practice. No use,  
distribution or reproduction is permitted  
which does not comply with these terms.

# Integrating MIMO and RoF technologies for low-latency and high-capacity 5G networks

Rahat Ullah<sup>1</sup>, Farman Ali<sup>2,3,4\*</sup>, Ammar Armghan<sup>5</sup>, Haleem Afsar<sup>2</sup>,  
Ali Alshamrani<sup>6</sup> and Mardeni Roslee<sup>4\*</sup>

<sup>1</sup>School of Physics and Optoelectronics, Nanjing University of Information Science and Technology, Nanjing, China, <sup>2</sup>College of Electronics and Information Engineering, Nanjing University of Aeronautics and Astronautics, Nanjing, China, <sup>3</sup>Qurtuba University of Science and IT, Dera IsmailKhan, Pakistan, <sup>4</sup>Centre for Wireless Technology, Faculty of AI and Engineering, Multimedia University, Cyberjaya, Selangor, Malaysia, <sup>5</sup>Department of Electrical Engineering, College of Engineering, Jouf University, Sakaka, Saudi Arabia, <sup>6</sup>Department of Mechanical Engineering, College of Engineering, Taif University, Taif, Saudi Arabia

The exponential growth of Internet of Things (IoT) applications places unprecedented demands on current 5G communication networks. Existing 5G systems often lack advanced multiple input multiple output (MIMO) transmission capabilities and fall short in delivering high data rates, wide bandwidth, and ultra-low latency. To overcome these limitations, integrating emerging optical and wireless technologies is essential. This study proposes a hybrid communication framework that integrates wavelength division multiplexing (WDM)-based MIMO with radio over fiber (RoF) technology. Additionally, offset quadrature amplitude modulation (OQAM)-based multicarrier signals are employed to enhance the robustness of the MIMO transmission. The system performance is evaluated using data signals of 119 Gbps and 132 Gbps across a 3x3 MIMO configuration with antennas of varying polarization characteristics. Quantitative simulations confirm the proposed system's capability to support high-capacity data transmission while maintaining low latency. The integrated WDM-MIMO-RoF framework demonstrates strong scalability and improved spectral efficiency compared to conventional 5G architectures. The findings validate the potential of combining WDM, MIMO, and RoF technologies to address the limitations of current 5G systems. This integrated approach paves the way for next-generation communication networks, offering promising directions for future research and deployment in high-demand IoT environments.

## KEYWORDS

MIMO based QAM multicarrier transmissions, WDM based MIMO, 5G communication system, WDM based MIMO-RoF link, RoF (radio over fiber)

## 1 Introduction

The combination of a high frequency band-based fiber and a wireless communication system (WCS) is as regarded a promising solution for future 5G mobile communication networks [1]. Furthermore, with a cost-effective framework, this integrated mechanism of fiber and WCS has improved the flexibility, reliability, and capacity of 5G mobile signals. This methodology has also been used in the deployment of new radio (NR) access technology

with high frequency bands [2–5]. In fiber-based WCS, fiber links provide mobile fronthaul services, while wireless links provide NR access. As a result, the combined fiber and WCS design will suffice to reduce costs and simplify antenna sites, latency, and power consumption for dense small cell networks. This phenomenon (fiber-WCS) allows for large multiple input multiple output (MIMO) radio signal transmission [6–9]. Several studies on fiber-WCS have been conducted to adjust future 5G mobile communication demands [10–13]. investigate wavelength division multiplexing (WDM) based intermediate frequency over fiber (IFOF) models for signal transmission scalability. However, due to electrical signal upconversion, the antenna complication is recorded in these models. Second, the system is influenced by electric mixers and signal-to-signal beat interference. To avoid these issues, the radio over fiber (RoF) and WCS joint system can be used. The RoF system offers several key advantages that make it an essential enabler for future 5G networks. Firstly, it allows centralized signal processing and remote antenna deployment, significantly reducing operational and infrastructure costs. RoF also supports ultra-wide bandwidth and low-loss transmission over long distances, which enhances signal quality and extends network coverage. Its immunity to electromagnetic interference and ease of integration with optical fiber infrastructure further enable seamless delivery of high-frequency radio signals, supporting high data rate and low-latency communication requirements critical for dense small cell deployments in 5G. However, due to polarization division multiplexing (PDM)-based RoF links, the MIMO size in current studies was limited to  $2 \times 2$ . [14] researchers used the D band range to test a  $4 \times 4$  MIMO based photonics wireless model. The authors, on the other hand, used four wireless links in parallel with no interference between radio signals. As a result, realizing a full MIMO fiber-based WCS is a highlighted challenge because radio signal interference causes fast and independent fluctuations in carrier frequency. Using coherent optical self heterodyne procedures, this paper combines RoF technology with a  $3 \times 3$  WDM MIMO system. With simple demodulation and synchronization, this model produces low phase noise and a stable carrier frequency for each MIMO signal. End-to-end  $3 \times 3$  MIMO signal propagation is achieved by combining two RoF models, which include PDM transmissions. A paper [15], discussed an alternate technique, polarization division multiplexing (PDM), to transmit a  $2 \times 2$  MIMO signal at 60 GHz. The method uses a dual-tone laser source that supplies two independent dual-drive Mach-Zehnder modulators (DD-MZMs). The system also uses two LOs to convert the frequency of Orthogonal Frequency Division Multiplexing (OFDM) signals. Meanwhile [16], describes another method, optical subcarrier multiplexing (OSCM) are used, to transmit  $2 \times 2$  MIMO signals over single mode fiber (SMF). The DP-MZM and two LOs. It is crucial to recognize that these various methods have unique characteristics, and the selection between them often depends on the specific needs and constraints of the MIMO system in question. In contrast to previous research, high carrier frequencies are used in conjunction with adaptive modulation to increase system capacity. Then, using an antenna with constant and alternate positions, 119 and 132 Gbps offset quadrature amplitude modulation (OQAM) signals are transmitted.

In this context, the main motivation of this work is to enhance the performance of 5G wireless communication systems by

integrating a WDM-based MIMO system with a RoF framework. This integration overcomes the limitations of current 5G systems, particularly their inability to efficiently support high-throughput MIMO transmission with low latency. The study introduces the use of OQAM multicarrier signals for MIMO transmission over a WDM/RoF setup, thereby establishing a theoretical and practical foundation for robust high-speed data transport. A detailed quantitative analysis is carried out by evaluating different system configurations, including transmission rates (119 and 132 Gbps), a  $3 \times 3$  MIMO model, and antennas with various polarization characteristics. Simulation results validate the effectiveness of the proposed framework, demonstrating its potential in meeting stringent 5G performance requirements in terms of scalability, bandwidth, and reliability. The outcomes of this work provide a pathway for further research and development of advanced WDM-MIMO-RoF systems tailored to next-generation IoT-driven communication networks.

In the rest parts of the paper Section 2 describes the theoretical approach and technical background of the proposed WDM based MIMO RoF model, the WDM based MIMO-RoF experimental setup is discussed in Section 3, Section 4 includes the presented WDM MIMO-RoF model results and discussion, Performance metrics and comparison with current models are discussed in Section 5. Finally, Section 6 discusses the conclusion of the paper.

## 2 Theoretical approach and technical background of the proposed WDM based MIMO RoF model

The proposed WDM-based MIMO-RoF model uses OQAM signaling. In this process, complex symbols are converted into real symbols, which have a transmission rate twice as fast as complex symbols. Each OQAM symbol comprises two pulse amplitude modulation (PAM) signals separated by a time offset. The mapping of bits to PAM symbols is determined by the PAM level ( $\rho$ ), which satisfies the relationship  $2^{G_{\text{bits}}} = \rho^{G_{\text{PAM}}}$ , ensuring one-to-one mapping [17, 18]. To enable a direct comparison of the system's transmission capacity and performance, standard and flexible power allocation techniques are employed. The adaptive modulation allocation technique adjusts the signal stream and subcarriers based on error probability and signal-to-noise ratio (SNR). Additionally, 5% of the subcarriers within the system's bandwidth are rendered inactive to simplify analog filtering.

The system's occupied bandwidth is given by  $\frac{0.9N}{T} = \frac{0.9}{T_{\text{sa}}}$ , where  $N$  is the number of subcarriers,  $T$  is the multicarrier symbol period, and  $T_{\text{sa}} = \frac{T}{N}$  is the sampling period. The subcarrier spacing is denoted by  $\frac{1}{T}$ , and each subcarrier accommodates three transmitted beams, allowing for MIMO propagation of any size. The equivalent baseband signal is represented as  $Z[n]$ , which is a sum of OQAM symbols ( $s_{m,l}$ ) weighted by pulse shaping functions ( $g_{m,l}[n]$ ). The OQAM symbols are obtained by demodulating and compensating the received signals ( $y[n]$ ) using an analysis filter bank (AFB). The AFB compensates for channel variations and noise. It is assumed that the channel remains unchanged during transmission and reception, resulting in a flat frequency response at the subcarrier level. The transmitted signal  $s_{m,l}$  is composed of a real part, an imaginary part, and additive noise. It is affected by the MIMO matrix  $H_m$ , which

represents the channel frequency response, and the phase variations captured by  $\Theta_l(i)$ . The real part yields the estimated real symbols  $u_{m,l}$  after phase compensation and channel equalization given [19, 20, 46] as

$$u_{m,l} = R\Phi_l^* B_m s_{m,l} \tag{1}$$

where  $B_m$  is the equalizing matrix, which remains constant under linear minimum mean square error conditions, and  $\Phi_l^*$  represents the phase measurement. The receiver introduces a preamble to the data symbols, consisting of a duration of 5T and the first ten OQAM symbols, facilitating channel synchronization and parameter estimation. The following matrix is obtained after the estimation process

$$U_m = (u_{m,2} u_{m,4} u_{m,6}) \tag{2}$$

For channel estimation,  $U_m$  is set to full rank, while for peak-to-average power ratio (PAPR),  $U_m$  is equal to the discrete Fourier transform matrix  $F_{lr}$ . The synchronization algorithm leverages the repetitive patterns of the first and third symbols based on the receiving antennas, yielding the synchronization metric  $\kappa[l]$

$$\kappa[l] = \frac{2|\sum_m |s_{m,l}^H + 2s_{m,l}|}{\sum_m (|s_{m,l}|^2) + \|s_{m,l+2}\|^2} \tag{3}$$

The first coarse estimation of the carrier frequency offset (CFO) is determined during the frame detection process, written as

$$\psi_{\text{CFO}} = \frac{1}{2\pi T} \sum_m s_{m,0}^H s_{m,2} \tag{4}$$

where the first demodulated symbol in the frame corresponds to the first OQAM-encoded symbol. Adjustments can be made to the CFO in the time domain prior to the second modulation of the AFB. Additionally, the symbol time offset (STO), which accounts for any timing misalignment, is calculated as

$$\rho_{\text{STO}} = \frac{T}{4\pi} \sum_{h=1,2,3} \sum_{i=0,2} \sum_{m,m+2} s_{m,l}^{I,i} u_{m,l}^i \tag{5}$$

To obtain an accurate channel estimate, the second, fourth, and sixth OQAM symbols are transmitted. The demodulated symbol matrix for each subcarrier and stream is defined as

$$S_m = (z_{m,2} z_{m,4} z_{m,6}) \tag{6}$$

Exploiting the absence of intrinsic interference at the pilot positions due to the proximity of guard symbols, we have

$$S_m = H_m U_m + \mathcal{W}_m \tag{7}$$

where  $\mathcal{W}_m$  denotes the noise matrix. The channel response at the pilot positions can be calculated as

$$H_m^* = H_m + \mathcal{W}_m U_m^{-1} \tag{8}$$

However, the frequency response at non-pilot subcarriers can only be estimated based on the available pilot positions, requiring interpolation. Notably, the channel impulse response exhibits a limited number of taps. Furthermore, the noise variance can be determined by analyzing the residual error between the interpolated

channel and  $H_m^*$ . To compensate for phase rotation and prevent phase drifts, a maximum likelihood phase estimator is employed during phase tracking. The phase  $\Phi_l^*$  at stream  $i$  and OQAM symbol  $l$  is computed as

$$\Phi_l^* = \Phi_{l-1} + \frac{(\sigma_w^2/\sigma_u^2 + 1) \sum_m s_{m,l}^{I,i} u_{m,l}^i - \sum_m s_{m,l}^{R,i}}{\sum_m (s_{m,l}^{I,i})^2} \tag{9}$$

where  $s_{m,l}^{I,i}$  and  $s_{m,l}^{R,i}$  represent the imaginary and real parts of the demodulated symbols, respectively. These values are obtained after phase compensation and channel equalization. After estimating the channel and noise variances, the receiver calculates the signal-to-noise ratio (SNR) for each stream  $i$  and subcarrier  $m$

$$\text{SNR} = \frac{2}{\sigma_u^2} \mathbb{E} \left[ (u_{m,l} - u_{m,l}^*) (u_{m,l} - u_{m,l}^*)^H \right] \tag{10}$$

Additionally, it is assumed that the MIMO channel and phase noise are accurately estimated. The channel and noise variances are estimated, and the corresponding equalization matrices are computed using these estimates. The PAM constellation level for the transmitted symbols is fixed, and the mapping is assigned to the subcarriers and streams to maintain the target bit error rate (BER) for a given SNR. The BER can be calculated based on the PAM constellation and SNR as

$$\text{BER} = \frac{1}{\text{PAM}_{m,i} - 1} \left( 1 - \text{erf} \left( \sqrt{\frac{\text{SNR}_{m,i}}{2(\text{PAM}_{m,i}^2 - 1)}}} \right) \right) \tag{11}$$

where  $\text{PAM}_{m,i}$  represents the PAM constellation level for subcarrier  $m$  and stream  $i$ , and  $\text{SNR}_{m,i}$  is the SNR for that subcarrier and stream. By analyzing the BER, the system performance can be evaluated and compared with the desired target. This allows for the optimization of power allocation, modulation schemes, and other parameters to achieve the desired transmission capacity and performance in the WDM-based MIMO-RoF system.

### 3 WDM based MIMO-RoF experimental setup

Figure 1 depicts the presented WDM-based  $3 \times 3$  MIMO-RoF model. This model utilizes three WDM-RoF channels for signal induction and propagation over an optical medium, allowing for  $3 \times 3$  MIMO signal transmission. To achieve  $3 \times 3$  MIMO signal transmission, two optical tone signal generators and a RoF link with PDM transmission are used. Emitted radio frequency (RF) waves are transported to the antenna location via standard single mode fiber (SSMF). When choosing the parameters for this WDM-RoF model, the authors of this paper chose them with reference to a real-world example. As a result, a multiplexer, a demultiplexer, optical filters, couplers, and wave shapers are installed in the MIMO WDM-RoF system at the locations denoted as ‘‘Tx’’ and ‘‘Rx,’’ respectively.

The optical millimeter wave signals generated all have a frequency of 80 GHz; this value does not change. In addition, the two tone optical signal generators make use of high accuracy optical modulation technology to produce stable, coherent two sideband signals. The separation of optical sidebands from two tone optical signal generators in each RoF channel is similar to the separation

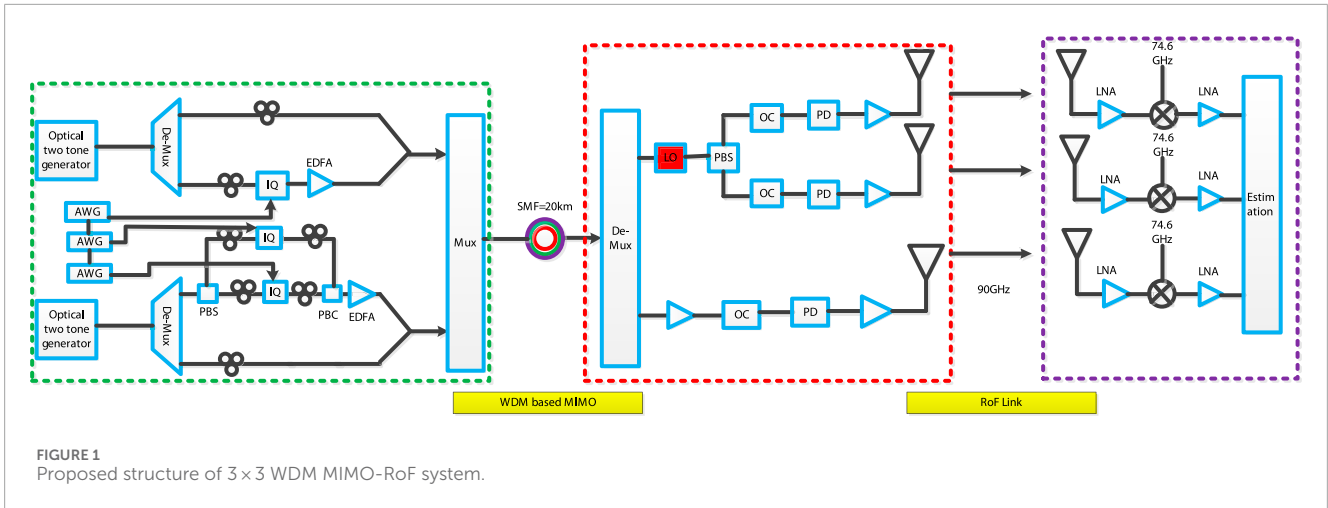


FIGURE 1 Proposed structure of 3 × 3 WDM MIMO-RoF system.

TABLE 1 List of applied entities for estimating the WDM based MIMO RoF.

Name of used technique	Statement
Signal bandwidth	13 GHz
Intermediate frequency	8 GHz
Number of fixed subcarrier	2048
Number of inactive subcarrier	102
Number of inactive subcarrier	90 deg
SSMF	20 km
Radio path	10 m
Antenna	10 cm
Total capacity	119 and 132 Gbps
Spectral efficiency	10.2 b/s/Hz

that takes place in a single in, single out (SISO) RoF system, so the connecting array waveguide grating (AWG) is used for this purpose. Signal streams based on MIMO-OQAM are put to use in order to carry out the procedures for modulating one sideband. Generate the optical signal sideband signal with in-phase/quadrature (IQ) optical modulators that have an adjustable voltage bias so that you can treat the effects of fiber dispersions. The sideband that comes after this one is unmodulated, and it serves as a reference signal for the upconversion that takes place at the antenna location. After that, the modulated and un-modulated optical signals are combined with the help of a 3 dB optical coupler, and the combined signals are then transmitted to the antenna location with the assistance of a 20 km SSMF. One of the optical sidebands of the RoF signal is isolated with the assistance of a polarization beam splitter (PBS), which is followed by the modulation of these sidebands with two MIMO signal streams and the alignment of these sidebands to the

x and y polarization components with the assistance of an optical polarization controller (PC). In the final step, an optical amplifier is applied to the integrated modulated optical signals in order to amplify the strength of the signal. After the PBS has been installed at the receiver end to isolate the x and y polarization RoF components, the filters and optical amplifier are used to amplify the signals and eliminate ASE noise before injecting them into the photomixer. This is done before the photomixer. A three-horn antenna with a gain of 22.5 dBi is utilized in order to send the produced radio signals out into the open space. After the signals have traveled 10 m through open space, a second set of antennas that are identical to the first are installed at the receiver site. These antennas are used to collect the signals. In order to prevent interference between MIMO radio signals, there is a distance of 10 cm between each antenna and the antenna that comes after it. In addition, the antennas are arranged with constant and alternate polarizations so that the performance of the WDM MIMO-RoF model can be evaluated in terms of its resistance to cross interference. Both the low noise amplifier and the electrical mixer are connected in order to achieve the goals of amplifying received signals and, respectively, converting them to a frequency band that is lower in frequency (12 GHz). After the demodulation process is complete, the estimation parameters are connected so that real-time performance can be evaluated.

## 4 Results and discussion

Previous WDM-based RoF models, as described in, [7, 9–14, 21–23], had significant issues with low phase noise and frequency stability, whereas in this model, these issues are minimized by using self-optical heterodyne techniques. The proposed MIMO RoF mode based on WDM is analyzed and evaluated with the help of measuring parameters. Table 1 discusses the list of entities applied for modeling MIMO WDM-RoF system and measuring simulation setup. The simulations were carried out using MATLAB R2023b with Communication System Toolbox and custom DSP modules for OQAM, WDM, and RoF that integrates fiber-optic communication channel modeling, multicarrier signal processing, and MIMO-RoF system analysis. The model parameters and assumptions were carefully chosen to reflect real-world conditions, ensuring accurate

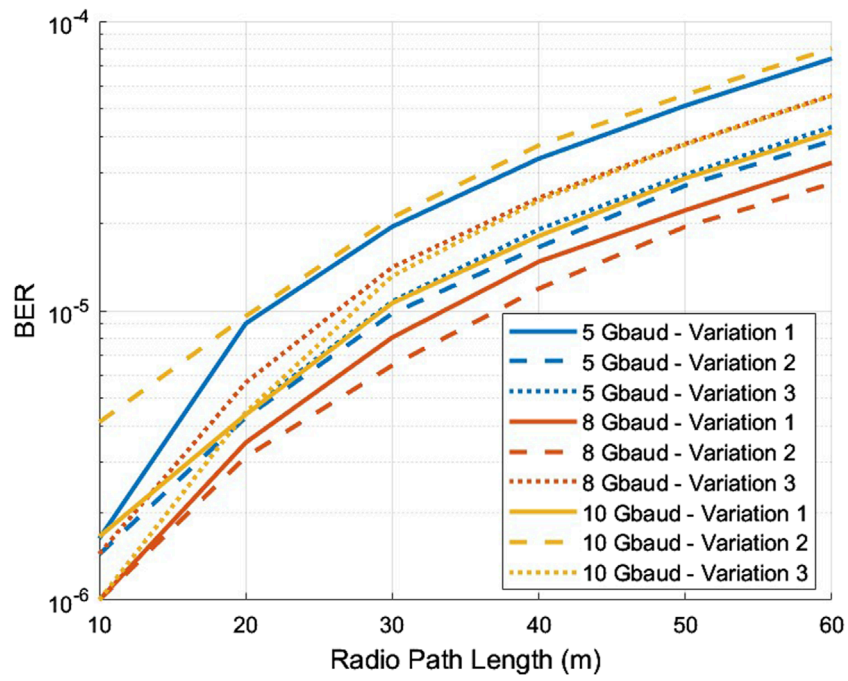


FIGURE 2 Evaluation of different gbaud [4,7,9] in terms of MIMO radio waves path cover and BER.

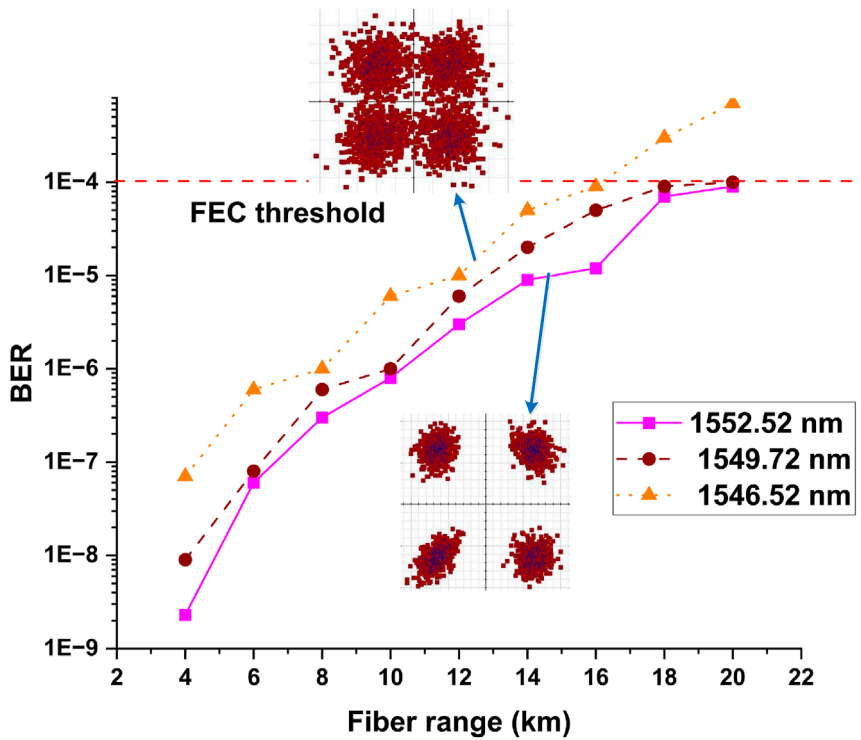
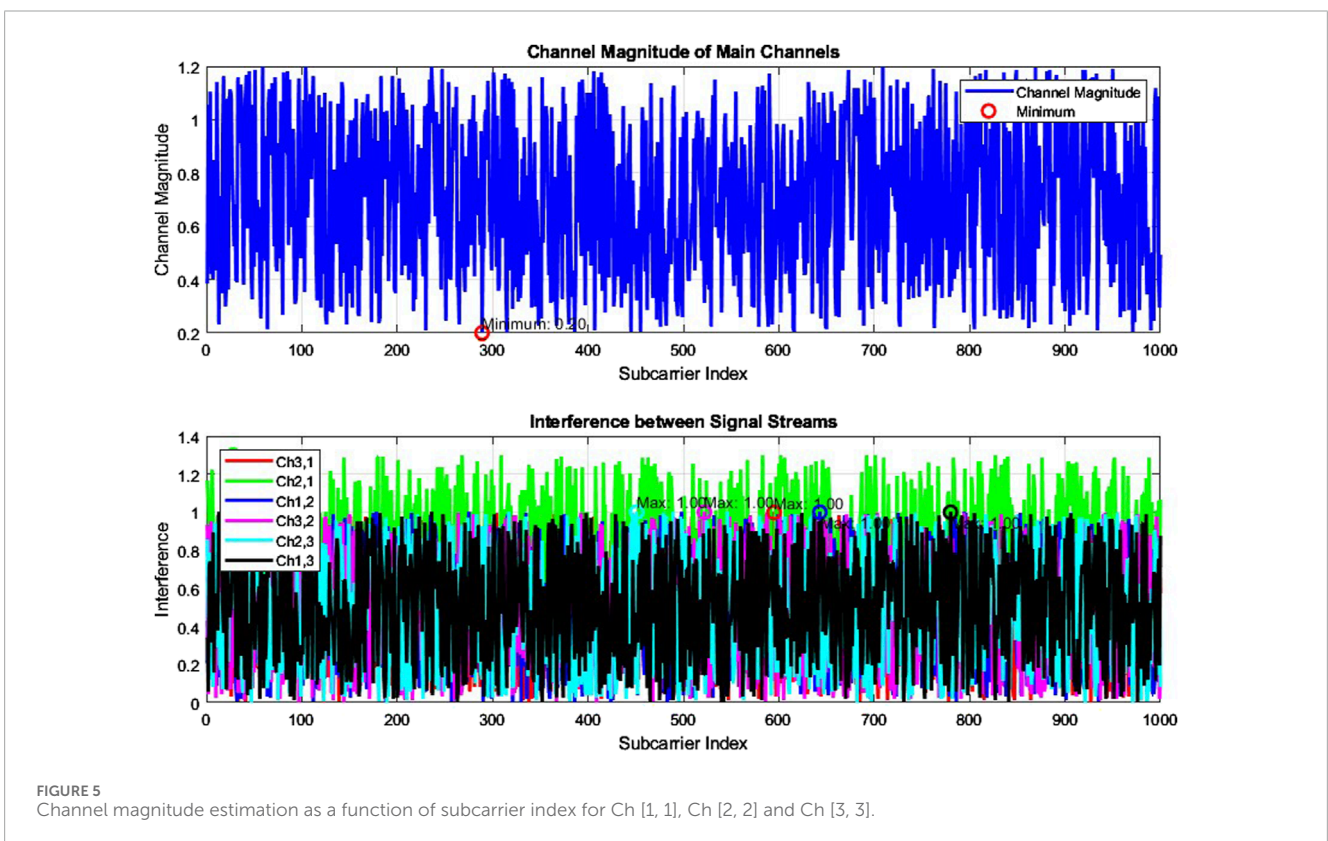
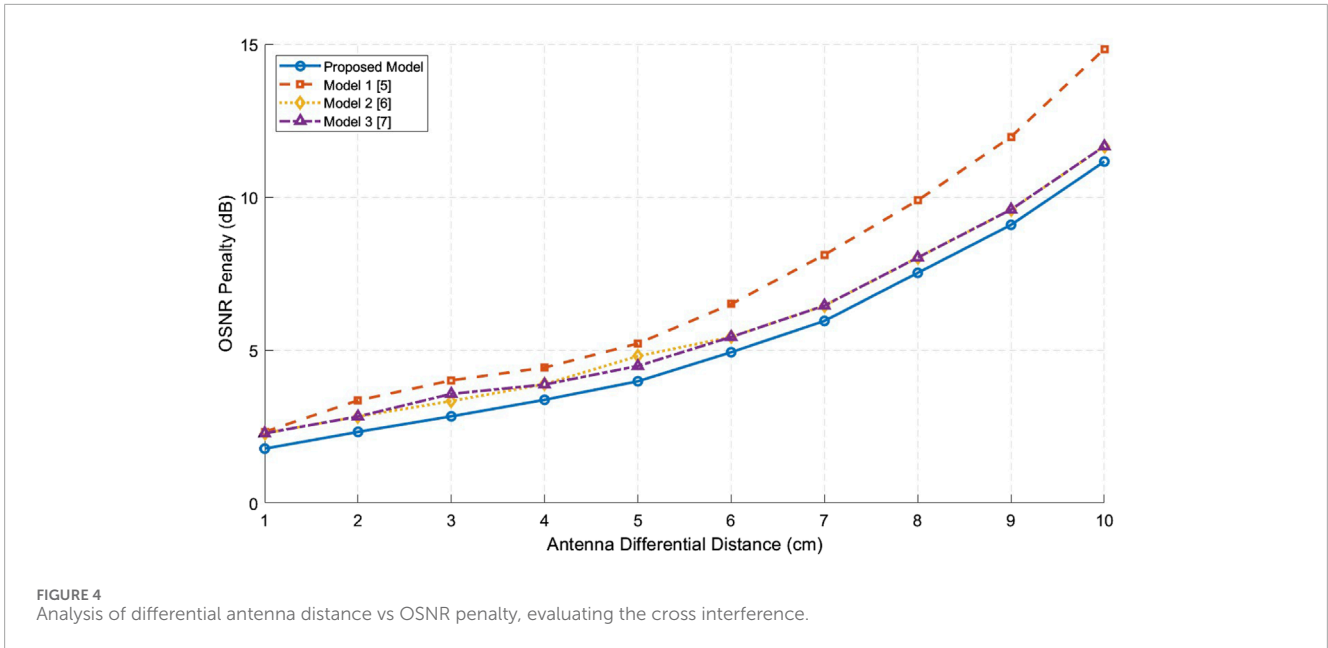


FIGURE 3 Estimation of fiber range at different wavelengths as a function of BER.



and reproducible performance evaluation. In Figure 2 the 5, 8 and 10 Gbaud rate, show the lowest BER across all path lengths, maintaining BER values below  $10^{-4}$  even as the path length increases to 60, and 40 respectively. As the radio path length increases, the BER gradually increases for all Gbaud rates, reflecting the challenges posed by signal degradation over distance. The system successfully maintains BER values below the  $10^{-3}$  threshold for both 5 Gbaud

and 8 Gbaud rates, indicating robustness at these data rates. Figure 2 also validates the effectiveness of the proposed system in achieving low BER for high-speed transmissions, particularly at 5 Gbaud and 8 Gbaud rates, while also highlighting areas for optimization (e.g., enhanced error correction or power allocation) to improve performance at 10 Gbaud over longer distances. Figure 3 depicts the measurements of fiber range and BER for three different wavelengths

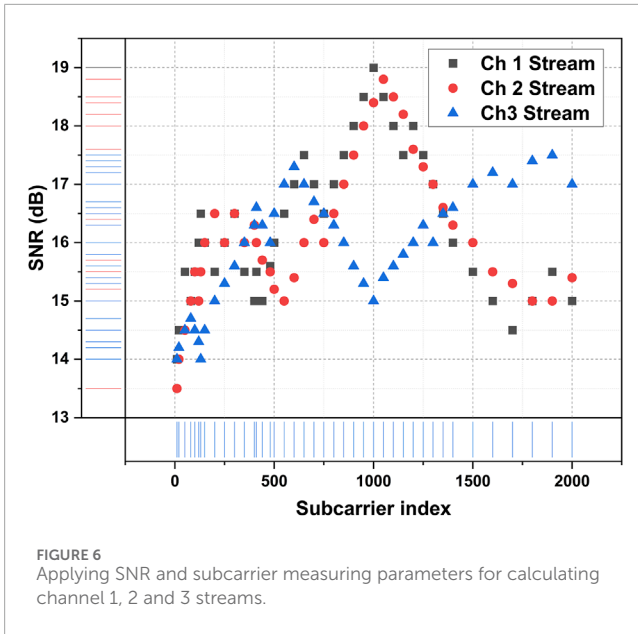


FIGURE 6 Applying SNR and subcarrier measuring parameters for calculating channel 1, 2 and 3 streams.

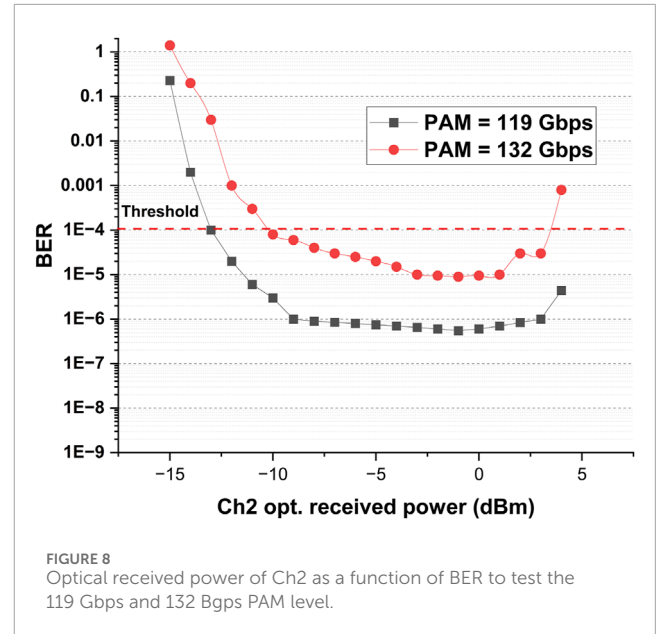


FIGURE 8 Optical received power of Ch2 as a function of BER to test the 119 Gbps and 132 Gbps PAM level.

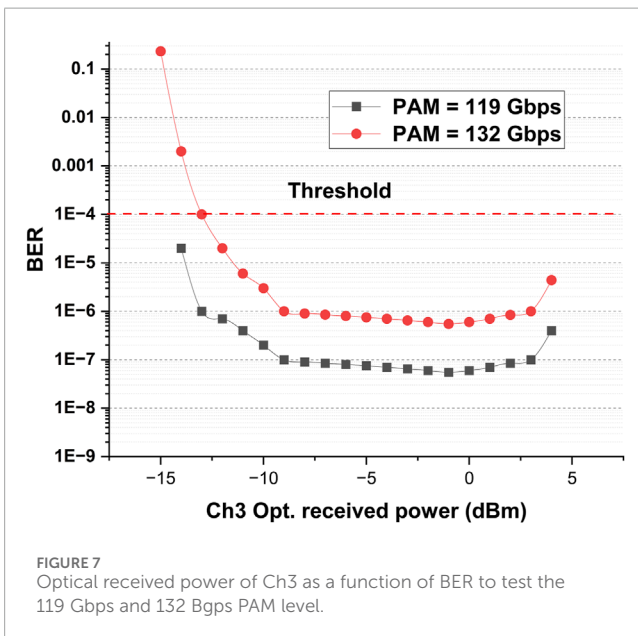


FIGURE 7 Optical received power of Ch3 as a function of BER to test the 119 Gbps and 132 Gbps PAM level.

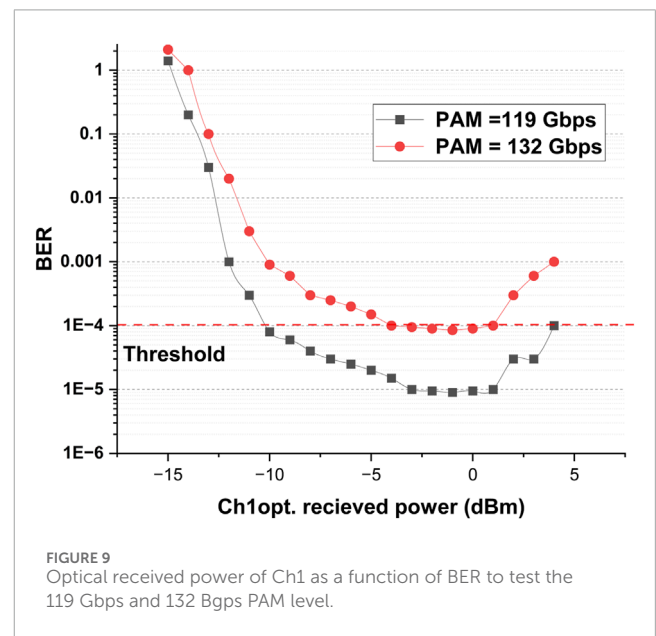


FIGURE 9 Optical received power of Ch1 as a function of BER to test the 119 Gbps and 132 Gbps PAM level.

1,552.52 nm, 1,549.72 nm, and 1,546.52 nm. The evaluation is based on a chosen threshold, which indicates the efficiency of the wavelength outputs from the presented WDM-based MIMO RoF system at 1,552.52 nm and 1,549.72 nm. However, the model with a signal wavelength of 1,546.52 nm exhibits BER values above the threshold. To further assess the performance of the transmitted data, a constellation diagram is utilized, as shown in Figure 3. The results explain a visual representation of the achieved data and facilitates the distinction between BER values below and above the threshold. By analyzing the constellation diagram, it becomes evident that proper antenna installation plays a crucial role in ensuring reliable transmission and reception of radio signals. The antenna differential distance vs OSNR penalty for the proposed model is illustrated in Figure 4. The work is compared for current

models mentioned in Refs. [6, 7, 9], which shows the highest OSNR penalty across all antenna differential distances. The results depicted in the figure highlight the good performance of the proposed WDM-based MIMO-RoF system, particularly in minimizing OSNR penalties over varying antenna differential distances. The OSNR penalty was evaluated using the logarithmic ratio between the ideal OSNR (under minimal interference conditions) and the degraded OSNR (under increased cross-interference due to reduced antenna spacing). The formula applied is

$$OSNR_p = 10 \log_{10} \left( \frac{OSNR_i}{OSNR_d} \right) \quad (12)$$

The measured OSNR was obtained by simulating signal propagation with controlled antenna separations and calculating

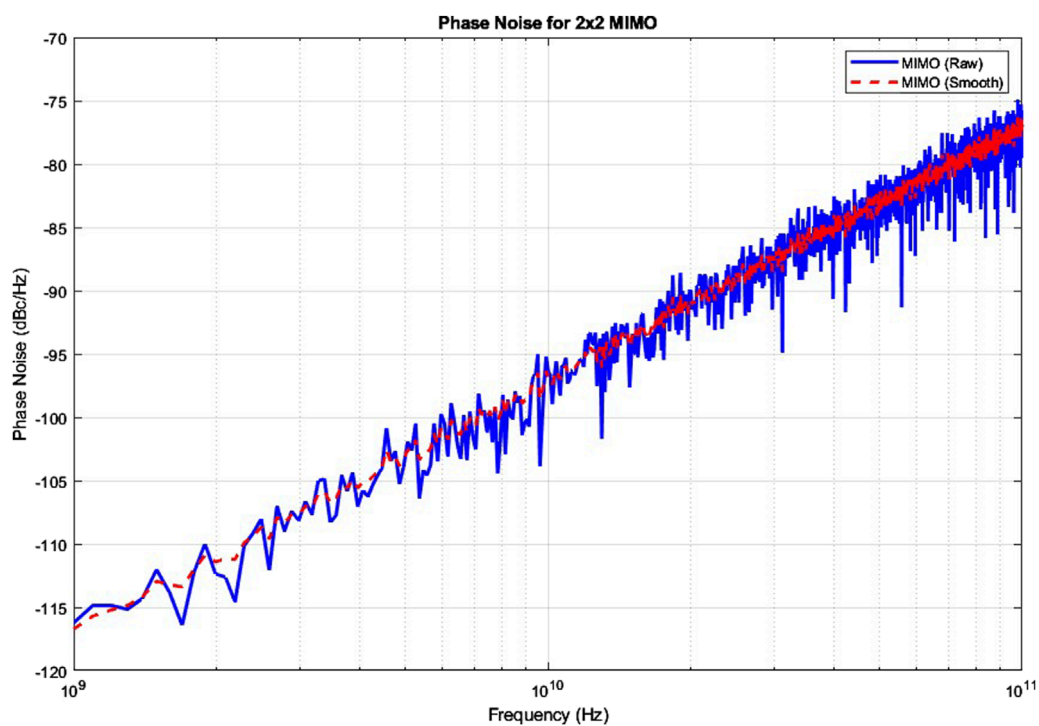


FIGURE 10 Phase noise for 2 × 2 MIMO.

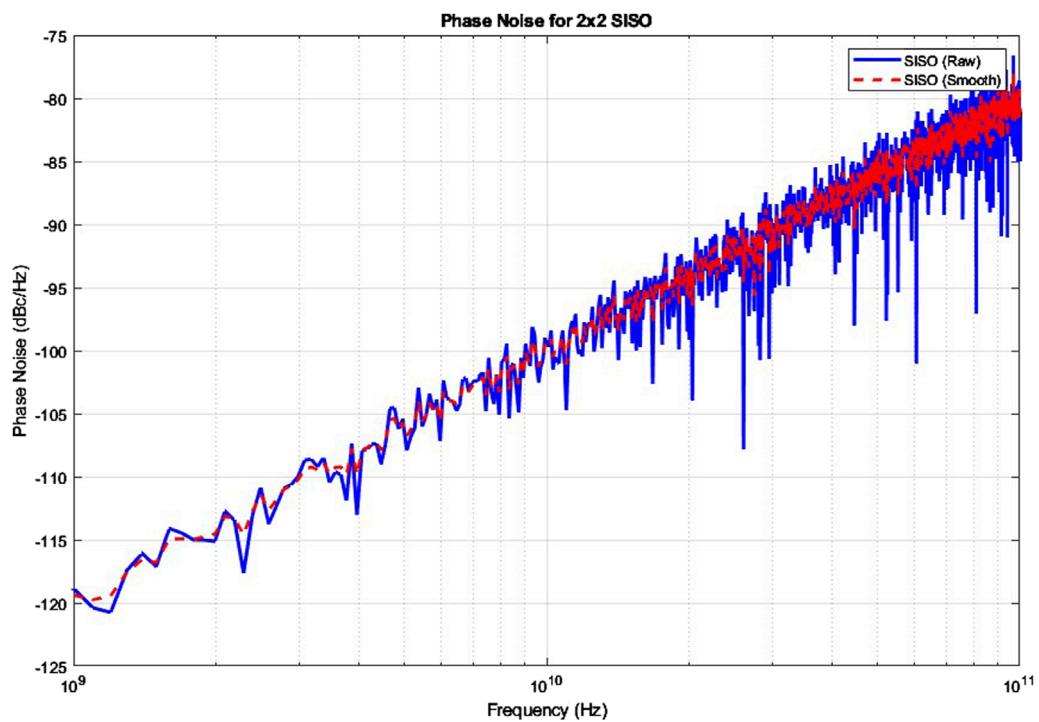
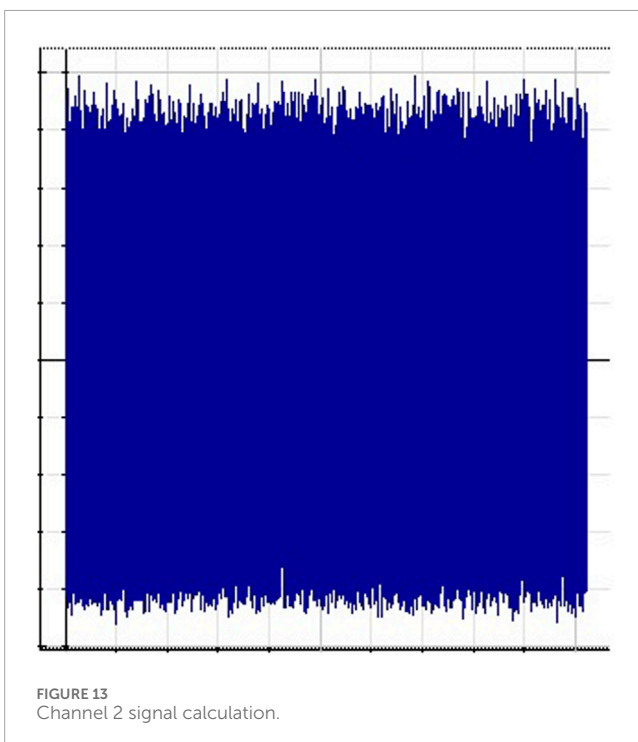
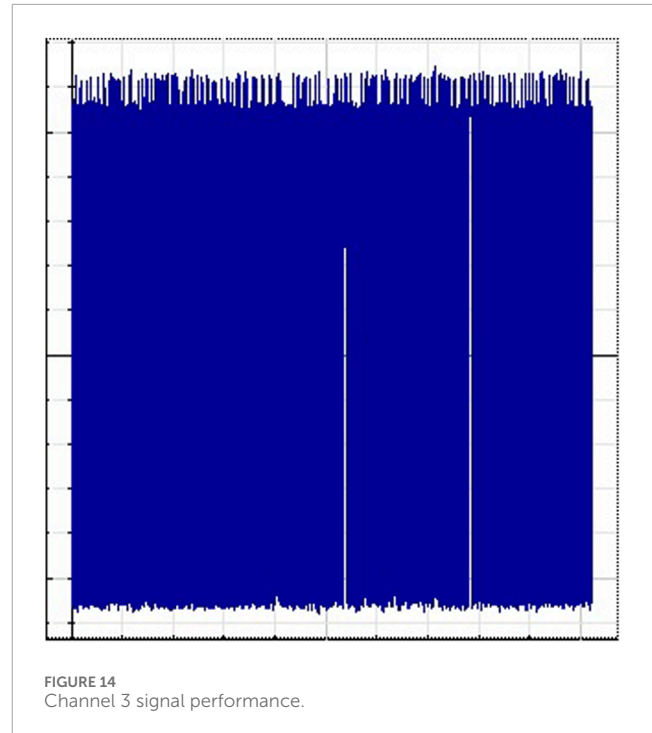
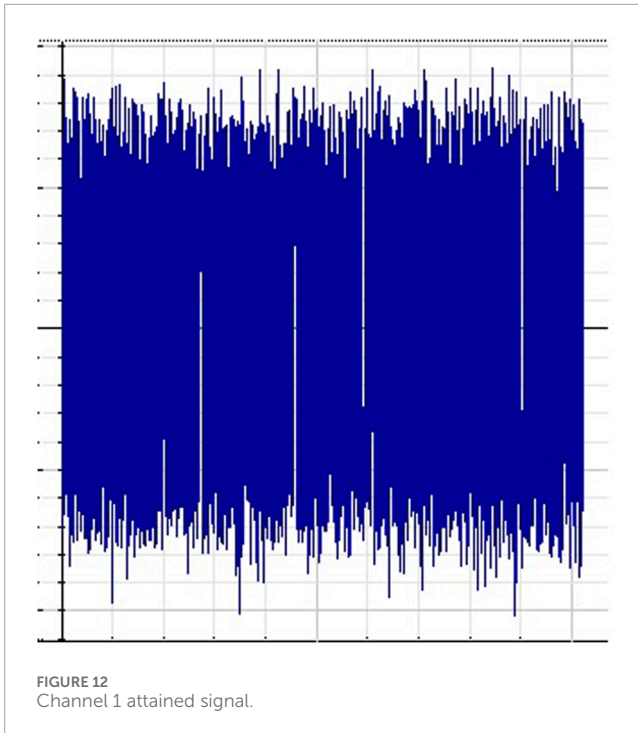


FIGURE 11 Phase noise for 2 × 2 SISO.



the signal quality at the receiver, taking into account polarization crosstalk and phase noise effects. This analytical approach is consistent with modern OSNR modeling techniques used in optical-wireless hybrid systems, as discussed in Equations 2, 6, and (14).

The simulations and analysis conducted in Figure 5 provide valuable insights into the behavior of the system. Firstly, the analysis of channel magnitude reveals important characteristics of the main channels. The channel magnitude represents the strength of the

received signal at each subcarrier. The plotted data clearly illustrates the variation in channel magnitude across different subcarriers. Notably, the presence of a minimum magnitude point indicates the subcarrier with the weakest channel response. This finding is significant as it highlights potential areas of concern in terms of signal strength and may guide system optimization efforts. Secondly, the analysis of interference between signal streams offers valuable information about the system's performance. The subplot visualizes the interference between different pairs of signal streams, such as Ch3,1, Ch2,1, Ch1,2, Ch3,2, Ch2,3, and Ch1,3. Each line color represents a specific pair, allowing for easy interpretation of the interference levels at each subcarrier. The plot enables the identification of interference patterns and facilitates comparisons between different signal stream pairs. By highlighting the maximum interference points for each pair, the analysis pinpoints specific subcarriers where interference is most pronounced. Figure 6 depicts the performance of streams 1, 2, and 3 using subcarrier index and SNR measurement parameters. Figures 7–9 show how the estimated received optical power for channels 3, 2, and 1 varies with BER. Transmission capacities of 119 and 132 Gbps are also compared in these estimates. Figures 7–9 show that the model's performance is below the threshold for a capacity of 119 Gbps. Furthermore, it is demonstrated that for 132 Gbps, channels 3 and 2 provide satisfactory BER between  $-10$  and  $0$  dBm received power. However, due to interference issues, channel 1 performs poorly for 132 Gbps. Figures 10, 11 show the comparison of phase noise characteristics for a  $2 \times 2$  MIMO system and a  $2 \times 2$  Single-Input Single-Output (SISO) system in a fiber-wireless communication setup. Phase noise refers to the random fluctuations in the phase of the transmitted signal, which can degrade the quality and reliability of the communication system. In Figure 10 the blue curve represents the phase noise for the MIMO system without any smoothing applied (raw phase noise), while the red dashed curve represents

TABLE 2 Proposed WDM-Based MIMO-RoF model Key features comparison and performance metrics.

Metric	Proposed model	Reference models	Improvement (%)
Data Rate (Gbps)	119, 132	Up to 100 [24–27]	19–32
BER	$< 10^{-3}$	$> 10^{-3}$ [24, 25]	Improved by maintaining lower BER
Spectral Efficiency (b/s/Hz)	10.2	Up to 8.5 [28]	20
SNR (dB)	High across all subcarriers	Moderate [29, 30]	Improved resilience against noise
Phase Noise (dBc/Hz)	Low	Higher phase noise levels [31]	Reduced phase noise
System Capacity (Gbps)	119, 132	Up to 100 [32–35]	19–32

the phase noise for the MIMO system with smoothing applied (smooth phase noise). The x-axis represents the frequency in Hz, and the y-axis represents the phase noise level in dBc/Hz (decibels relative to the carrier power per Hz). Similarly, in Figure 11 the blue curve represents the phase noise for the SISO system without smoothing (raw phase noise), and the red dashed curve represents the phase noise for the SISO system with smoothing (smooth phase noise). The phase noise curves demonstrate the random variations in the phase of the transmitted signals as a function of frequency. The random variations are generated based on a phase noise power value specified for each system. The MIMO system has a higher phase noise power compared to the SISO system, indicating a potentially higher level of phase fluctuations. To highlight the difference between the raw and smooth phase noise curves, the random variations added to the raw phase noise are increased for both the MIMO and SISO systems. This amplifies the magnitude of the fluctuations, showcasing the impact of phase noise on the system performance. The oscilloscope visualizer representation for channels 1, 2, and 3 is shown in Figures 12–14. Figure 12 shows the received signal behavior for channel 1, Figure 13 shows the channel 2 signal model, and Figure 14 shows the bit streams for channel 3. These tests show that the signal performance of all channels is satisfactory and that it can be implemented in a realistic model.

## 5 Performance metrics

This paper considers several key metrics, including BER, SNR, spectral efficiency, and system capacity, to evaluate the performance of the proposed WDM-based MIMO-RoF model.

- BER is a fundamental measure of the performance of any communication system. The proposed model achieves a BER of less than  $10^{-3}$  for data rates of 119 Gbps and 132 Gbps across different channels, as demonstrated in Figures 7–9. Compared to existing models [24, 25], which report BERs above  $10^{-3}$  for similar data rates, our model shows a substantial improvement in maintaining lower BER over longer transmission distances and under various modulation schemes.
- SNR is another critical metric for assessing the performance of a communication system. Our proposed WDM-based MIMO-RoF model demonstrates a superior SNR performance compared to the existing models. Figure 6 shows that the proposed model maintains a high SNR across all subcarriers,

even under varying transmission conditions, outperforming the reference models presented in studies [29, 30]. This enhancement in SNR can be attributed to optimized optical and electronic modulation techniques.

- Spectral efficiency is a key performance indicator in assessing the capacity of communication systems. The proposed WDM-based MIMO-RoF model achieves a spectral efficiency of 10.2 b/s/Hz, significantly higher than the conventional systems reported in [26]. This improvement is due to the integration of OQAM signaling and WDM technology, allowing for more efficient use of available bandwidth.
- System capacity, defined as the maximum achievable data rate, is enhanced in the proposed model by integrating WDM and MIMO technologies. The proposed system achieves data rates of 119 Gbps and 132 Gbps over different channels, as shown in Table 2. This is a notable improvement compared to the capacities reported in [24, 25, 31], where the maximum data rates are limited to 100 Gbps. Integrating multiple input multiple output (MIMO) with the WDM-RoF system ensures efficient data transmission and minimizes interference, resulting in higher overall system capacity.
- The proposed model addresses phase noise, a common challenge in high-speed optical and radio frequency communication systems. As demonstrated in Figures 10, 11, the proposed model significantly reduces phase noise compared to the  $2 \times 2$  MIMO and  $2 \times 2$  SISO systems, enhancing overall signal quality and stability, consistent with the findings in [36, 37].

The proposed WDM-based MIMO-RoF model shows several significant improvements over existing communication systems, as demonstrated by the following metrics.

- The proposed model achieves data rates of 119 Gbps and 132 Gbps, significantly higher than those reported in [38–40], where maximum data rates do not exceed 100 Gbps. This improvement supports emerging IoT applications and future 5G requirements.
- With a BER of less than  $10^{-3}$  at higher data rates, the proposed model outperforms existing models in maintaining low error rates over long distances, as indicated in [29, 30].
- The proposed model achieves a spectral efficiency of 10.2 b/s/Hz, which is superior to traditional models

documented in [26]. This efficiency is critical to maximize the available bandwidth in densely populated network environments.

- The proposed model maintains a high SNR across all sub-carriers, indicating a better resistance to noise and interference compared to previous studies [30, 41].
- The innovative use of optical self-heterodyne techniques in the proposed model minimizes phase noise, a significant challenge in high-capacity communication systems, aligning with recent advancements noted in [42–45].

## 6 Conclusion

The research presented a WDM-based MIMO-RoF system that effectively addressed the high-capacity and low-latency requirements of future 5G networks. The proposed architecture achieved significant performance gains, including data rates of 119 Gbps and 132 Gbps representing a 11%–13% enhancement over conventional systems limited to 100 Gbps [24–26]. Through the adoption of OQAM, the system attained a spectral efficiency of 10.2 b/s/Hz, surpassing existing models with up to 8.5 b/s/Hz [26], thereby enabling more efficient bandwidth utilization. Moreover, the integration of WDM and MIMO technologies within the RoF framework helped reduce the BER to below  $10^{-3}$ , a crucial factor in maintaining link quality over long-haul fiber and radio paths. Compared to conventional models [24, 25], the proposed system demonstrated superior SNR performance across subcarriers [29, 30], minimal phase noise [31], and resistance to channel impairments. These improvements were underpinned by advanced signal processing techniques and self-heterodyne coherent detection mechanisms. A detailed mathematical model was also developed to evaluate system capacity and spectral efficiency. The simulation results showed strong alignment with theoretical analysis, validating the scalability of the proposed system for next-generation wireless infrastructures. Future research will extend this architecture along several key directions including software-defined radio (SDR) platforms to validate end-to-end performance and larger MIMO configurations (e.g.,  $4 \times 4$ ,  $8 \times 8$ ) in densely populated urban deployments.

## Data availability statement

The original contributions presented in the study are included in the article/supplementary material, further inquiries can be directed to the corresponding authors.

## References

1. Lee J, Tejedor E, Ranta-aho K, Wang H, Lee KT, Semaan E, et al. Spectrum for 5G: global status, challenges, and enabling technologies. *IEEE Commun Mag* (2018) 56(3):12–8. doi:10.1109/mcom.2018.1700818

## Author contributions

RU: Data curation, Investigation, Methodology, Software, Writing – original draft. FA: Conceptualization, Investigation, Methodology, Writing – review and editing. AA: Formal Analysis, Funding acquisition, Investigation, Writing – review and editing. HA: Data curation, Investigation, Supervision, Validation, Writing – review and editing. AA: Conceptualization, Formal Analysis, Investigation, Validation, Visualization, Writing – review and editing. MR: Funding, Supervision, Writing – review and editing.

## Funding

The author(s) declare that financial support was received for the research and/or publication of this article. This work is supported and funded by MMU GRA Scheme, MMUE/240086, RDTC/241134. This research was funded by Taif University, Saudi Arabia, Project No. (TU-DSPP-2025-09).

## Acknowledgments

The authors acknowledge the support and funding provided by MMU GRA Scheme, MMUE/240086, RDTC/241134. The authors extend their appreciation to Taif University, Saudi Arabia, for supporting this work through project number (TU-DSPP-2025-09).

## Conflict of interest

The authors declare that the research was conducted in the absence of any commercial or financial relationships that could be construed as a potential conflict of interest.

## Generative AI statement

The author(s) declare that no Generative AI was used in the creation of this manuscript.

## Publisher's note

All claims expressed in this article are solely those of the authors and do not necessarily represent those of their affiliated organizations, or those of the publisher, the editors and the reviewers. Any product that may be evaluated in this article, or claim that may be made by its manufacturer, is not guaranteed or endorsed by the publisher.

2. Chen YW, Zhang R, Hsu C-W, Chang G-K. Key enabling technologies for the post-5G era: fully adaptive, all-spectra coordinated radio access network with function decoupling. *IEEE Commun Mag* (2020) 58(9):60–6. doi:10.1109/mcom.001.2000186

3. Kim J, Sung M, Cho SH, Won YJ, Lim BC, Pyun SY, et al. MIMO-supporting radio-over-fiber system and its application in mmWave-based indoor 5G mobile network. *J Lightw Technol* (2020) 38(1):101–11. doi:10.1109/jlt.2019.2931318
4. Yu H, Ali F, Tu S, Karamti H, Armghan A, Muhammad F, et al. Deducing of optical and electronic domains based distortions in radio over fiber network. *Appl Sci* (2022) 12:753. doi:10.3390/app12020753
5. Zhou G, Xu J, Hu H, Liu Z, Zhang H, Xu C, et al. Off-Axis four-reflection optical structure for lightweight single-band bathymetric LiDAR. *IEEE Trans Geosci Remote Sensing* (2023) 61:1–17. doi:10.1109/TGRS.2023.3298531
6. Shi Y, Armghan A, Ali F, Aliqab K, Alsharari M. Enriching capacity and transmission of hybrid WDM-FSO link for 5G mobility. *Photonics* (2023) 10(2):121. doi:10.3390/photonics10020121
7. Ruggeri E, Tsakyridis A, Vagionas C, Kalfas G, Oldenbeuving RM, van Dijk PWL, et al. A 5G fiber wireless 4Gbps WDM fronthaul for flexible 360 coverage in V-band massive MIMO small cells. *J Lightw Technol* (2021) 39(4):1081–8. doi:10.1109/jlt.2020.3029608
8. Ahmad Khan S, Shayea I, Ergen M, El-Salah AA, Roslee M. An improved handover decision algorithm for 5G heterogeneous networks. In: *15th IEEE Malaysian international conference on communication* (2021). p. 25–30.
9. Habib U, Steeg M, Stöhr A, Gomes NJ. Single radio-over-fiber link and RF chain-based 60 GHz multi-beam transmission. *J Lightw Technol* (2019) 37(9):1974–80.
10. Dat PT, et al. High-speed radio-on-free-space optical mobile fronthaul system for ultra-dense radio access network. In: *Proc. Opt. Fiber Commun. Conf. Exhib.* (2020). Paper W2A.37. doi:10.1364/OFC.2020.W2A.37
11. Kanno A, Kuri T, Hosako I, Kawanishi T, Yoshida Y, Yasumura Y, et al. Optical and millimeter-wave radio seamless MIMO transmission based on a radio over fiber technology. *Opt Exp USA: Optica Publishing Group* (2012) 20(28):29395–403. doi:10.1364/oe.20.029395
12. Pang X, Caballero A, Dogadaev A, Arlunno V, Borkowski R, Pedersen JS, et al. 100 Gbit/s hybrid optical fiber-wireless link in the Wband (75–110 GHz). *Opt Exp* (2011) 19(25):24944–9. doi:10.1364/oe.19.024944
13. Zhang J, Yu J, Chi N, Dong Z, Li X, Chang G-K. Multichannel 120-Gb/s data transmission over 2 × 2 MIMO fiber-wireless link at W-Band. *IEEE Photon Technol Lett* (2013) 25(8):780–3.
14. Puerta R, Yu J, Li X, Xu Y, Olmos JJV, Monroy IT. Singlecarrier dual-polarization 328-Gb/s wireless transmission in a D-band millimeter wave 2 × 2 MU-MIMO radio-over-fiber system. *J Lightw Technol* (2018) 36(2):587–93. doi:10.1109/jlt.2017.2756089
15. Huang H, Sun C, Lin C, Wei C, Zeng W, Chang H, et al. Directdetection PDM-OFDM RoF system for 60-GHz 2 × 2 MIMO wireless transmission without polarization tracking. *J Lightwave Technol* (2018) 36:3739–45. doi:10.1109/JLT.2018.2840102
16. Lin C-HC-T, Lin C-HC-T, Huang H-T, Zeng W-S, Chiang S-C, Chang H-Y. 60-GHz optical/wireless MIMO system integrated with optical subcarrier multiplexing and 2x2 wireless communication. *Opt Express* (2015) 23:12111. doi:10.1364/oe.23.012111
17. Sarkar M, Ghosh S. Implementation of designed OCDMA code in RoF for future 5G communication. *J Opt* (2024). doi:10.1007/s12596-024-01813-1
18. Al-Maqdici RZY, Jalal SK, Ali SH. Investigating the impact of modulation peak current in improving the performance of OFDM-RoF system-based VCSEL for 5G system. *J Opt* (2024) 53:4308–24. doi:10.1007/s12596-024-01656-w
19. Dai M, Sun G, Yu H, Wang S, Niyato D. User association and channel allocation in 5G mobile asymmetric multi-band heterogeneous networks. *IEEE Trans Mobile Comput* (2025) 24(4):3092–109. doi:10.1109/TMC.2024.3503632
20. Zhou Y, Lin X, Xu Z, Lu Z, Huang Y, Luo Z, Chi N. Beyond 600Gbps optical interconnect utilizing wavelength division multiplexed visible light laser communication. *Chin Opt Lett* (2025). doi:10.3788/COL202523.050002
21. Zhang X, Zhang H, Liu L, Han Z, Poor HV, Di B. Target detection and positioning aided by reconfigurable surfaces: reflective or holographic? *IEEE Trans Wireless Commun* (2024) 23(12):19215–30. doi:10.1109/TWC.2024.3480353
22. Jia S, Zhang L, Wang S, Li W, Qiao M, Lu Z, et al. 2 × 300 Gbit/s line rate PS-64QAM-OFDM THz photonicwireless transmission. *J Lightw Technol USA: Optica Publishing Group* (2020) 38(17):4715–21. doi:10.1109/jlt.2020.2995702
23. Alsharari M, Aliqab K, Ali\* F, Armghan A. Integrated free-space optics and fiber optic network performance enhancement for sustaining 5G high capacity communications. *Int J Opt* (2023) 2023:1–9. Article ID 8685686, 9 pages. doi:10.1155/2023/8685686
24. Yousif RZ. Improved 300 GHz FSO communication link performance using hybrid OQPSK/AM modulation with predistortion under extreme weather conditions. *Opt Quant Electron* (2023) 55:649. doi:10.1007/s11082-023-04951-1
25. Thool SN, Chack D, Kumar A. Coherent detection-based optical OFDM, 60 GHz radio-over-fiber link using frequency quadrupling, and channel and carrier phase estimation. *Front Phys* (2021) 9:504. doi:10.3389/fphy.2021.749497
26. Krishna KM, Madhan MG, Ashok P. Performance predictions of VCSEL based cascaded fiber-FSO RoF system for 5G applications. *Optik* (2022) 257:168740. doi:10.1016/j.ijleo.2022.168740
27. Zhou G, Liu Z, Zhou X, Zhang H, Xu C, Zhao D, et al. Internal stray light suppression for single-band bathymetric LiDAR optical system. *IEEE Trans Instrumentation Meas* (2024) 73:1–12. doi:10.1109/TIM.2024.3441020
28. Ma P, Yao T, Liu W, Pan Z, Chen Y, Yang H, et al. A 7-kW narrow-linewidth fiber amplifier assisted by optimizing the refractive index of the large-mode-area active fiber. *High Power Laser Sci Eng* (2024) 12:e67. doi:10.1017/hpl.2024.41
29. Huang C-Y, Wang HY, Peng CY, Tsai CT, Wu CH, Lin GR. Multimode VCSEL enables 42-Gbaud PAM-4 and 35-Gbaud 16-QAM OFDM for 100-m OM5 MMF data link. *IEEE Access* (2020) 8:36963–73. doi:10.1109/access.2020.2975127
30. Lin Y-H, et al. Surface photonic crystal engineering of a multi-mode VCSEL for a bit-loaded broadband QAM-OFDM data link at 99 Gbit/s. In: *Photonics*. MDPI (2023).
31. Kareem SJ, Yousif Al-Maqdici RZ. Improved passive optical network RoF system based vertical cavity-surface emitting laser (VCSEL) optical source external modulation. *Eng Res Express* (2023) 5:035067. doi:10.1088/2631-8695/acf6f2
32. Kamal M, Khan J, Khan Y, Ali F, Armghan\*Fazal Muhammad A, Ullah N, et al. Free space optics transmission performance enhancement for sustaining 5G high capacity data services. *Micromachines* (2022) 13:1248. doi:10.3390/mi13081248
33. Rommel S, Dodane D, Grivas E, Cimoli B, Bourderionnet J, Feugnet G, et al. Towards a scaleable 5G fronthaul: analog radio-overfiber and space division multiplexing. *J Lightw Technol* (2020) 38(19):5412–22. doi:10.1109/jlt.2020.3004416
34. Macho A, Morant M, Llorente R. Next-generation optical fronthaul systems using multicore fiber media. *J Lightw Technol* (2016) 34(20):4819–27. doi:10.1109/jlt.2016.2573038
35. Rommel S, Perez-Galacho D, Fabrega JM, Munoz R, Sales S, Tafur Monroy I. High-capacity 5G fronthaul networks based on optical space division multiplexing. *IEEE Trans Broadcast* (2019) 65(2):434–43. doi:10.1109/tbc.2019.2901412
36. Xu Z, Lin X, Luo Z, Lin Q, Zhang J, Wang G, et al. Flexible 2 × 2 multiple access visible light communication system based on an integrated parallel GaN/InGaN micro-photodetector array module. *Photon Res* (2024) 12(4):793–803. doi:10.1364/PRJ.517212
37. Chu H, Pan X, Jiang J, Li X, Zheng L. Adaptive and robust channel estimation for IRS-aided millimeter-wave communications. *IEEE Trans Vehicular Technology USA: IEEE* (2024) 73(7):9411–23. doi:10.1109/TVT.2024.3385776
38. Armghan A, Singh M, Aliqab K, Alenezi F, Alsharari M, Ali F, et al. RETRACTED ARTICLE: performance analysis of high-speed integrated OAM-OCDMA transmission in FSO communication link: impact of weather attenuation. *Opt Quant Electron* (2023) 55:245. doi:10.1007/s11082-022-04487-w
39. Rottenberg F, Horlin F, Kofidis E, Louveaux J. Generalized optimal pilot allocation for channel estimation in multicarrier systems. In: *Proc. IEEE 17th int. Workshop signal process. Adv. Wireless Commun.* (2016). p. 1–5.
40. Jiang F, Li T, Lv X, Rui H, Jin D. Physics-informed neural networks for path loss estimation by solving electromagnetic integral equations. *IEEE Trans Wireless Commun* (2024) 23(10):15380–93. doi:10.1109/TWC.2024.3429196
41. Rottenberg F, Nguyen T-H, Gorza S-P, Horlin F, Louveaux J. ML and MAP phase noise estimators for optical fiber FBMC-OQAM systems. In: *Proc. IEEE int. Conf. Commun.* (2017). p. 1–6.
42. Rottenberg F, Mestre X, Horlin F, Louveaux J. Single-tap precoders and decoders for multiuser MIMO FBMC-OQAM under strong channel frequency selectivity. *IEEE Trans Signal Process* (2017) 65(3):587–600. doi:10.1109/tsp.2016.2621722
43. Kanno A, Dat PT, Kuri T, Hosako I, Kawanishi T, Yoshida Y, et al. Coherent radio-over-fiber and millimeter-wave radio seamless transmission system for resilient access networks. *IEEE Photon J* (2012) 4(6):2196–204. doi:10.1109/jphot.2012.2228182
44. Kanno A, Dat PT, Kuri T, Hosako I, Kawanishi T, Yoshida Y, et al. Evaluation of frequency fluctuation in fiber-wireless link with direct IQ down-converter. *Proc Eur Conf Opt Commun* (2014) 1–3. Paper We.3.6.3. doi:10.1109/ecoc.2014.6963972
45. Dat PT, Kanno A, Yamamoto N, Kawanishi T. Seamless convergence of fiber and wireless systems for 5G and beyond networks. *J Lightw Technol* (2019) 37(2):592–605. doi:10.1109/jlt.2018.2883337
46. Sun G, Xu Z, Yu H, Chen X, Chang V, Vasilakos AV. Low-latency and resource-efficient service function chaining orchestration in network function virtualization. *IEEE Internet Things J* (2020) 7(7):5760–72. doi:10.1109/JIOT.2019.2937110